Mitochondrial Function and Nuclear Factor-κB–Mediated Signaling in Radiation-Induced Bystander Effects

Hongning Zhou,[1] Vladimir N. Ivanov,[1] Yu-Chin Lien,[1] Mercy Davidson,[2] and Tom K. Hei[1,3]

[1]Center for Radiological Research, [2]Department of Neurology, College of Physicians and Surgeons, and [3]Department of Environmental Health Science, Mailman School of Public Health, Columbia University, New York, New York

Abstract

Although radiation-induced bystander effects have been well described over the past decade, the mechanisms of the signaling processes involved in the bystander phenomenon remain unclear. In the present study, using the Columbia University charged particle microbeam, we found that mitochondrial DNA–depleted human skin fibroblasts (ρ^o) showed a higher bystander mutagenic response in confluent monolayers when a fraction of the same population were irradiated with lethal doses compared with their parental mitochondrial–functional cells (ρ^+). However, using mixed cultures of ρ^o and ρ^+ cells and targeting only one population of cells with a lethal dose of α-particles, a decreased bystander mutagenesis was uniformly found in nonirradiated bystander cells of both cell types, indicating that signals from one cell type can modulate expression of bystander response in another cell type. In addition, we found that Bay 11-7082, a pharmacologic inhibitor of nuclear factor-κB (NF-κB) activation, and 2-(4-carboxyphenyl)-4,4,5,5-tetramethylimidazoline-1-oxyl-3-oxide, a scavenger of nitric oxide (NO), significantly decreased the mutation frequency in both bystander ρ^o and ρ^+ cells. Furthermore, we found that NF-κB activity and its dependent proteins, cyclooxygenase-2 (COX-2) and inducible NO synthase (iNOS), were lower in bystander ρ^o cells when compared with their ρ^+ counterparts. Our results indicated that mitochondria play an important role in the regulation of radiation-induced bystander effects and that mitochondria-dependent NF-κB/iNOS/NO and NF-κB/COX-2/prostaglandin E2 signaling pathways are important to the process. [Cancer Res 2008;68(7):2233–40]

Introduction

Radiation-induced bystander effect is defined as the induction of biological effects in cells that are not directly traversed by a charged particle but are receiving signals from the irradiated cells that are in close proximity to them. Although the bystander effects have been well described over the past decade (1–4), the precise mechanisms of the process remain unclear. In subconfluent cultures, there is evidence that reactive oxygen species (ROS), nitric oxide (NO), and cytokines, such as transforming growth factor β, are involved in mediating the process (5–9). On the other hand, gap junction–mediated cell-cell communications have been shown to be critical for bystander effects in confluent cultures of either human or rodent origins (10–13). It is likely that a combination of pathways involving both primary and secondary signaling processes is involved in producing a bystander effect.

Using primary human fibroblasts, we showed previously that the cyclooxygenase-2 (COX-2) signaling cascade, including the activation of mitogen-activated protein kinase (MAPK) pathways, plays an essential role in the bystander process (14). Because COX-2 is often induced after treatment with growth factors and cytokines, such as tumor necrosis factor α (TNFα), we further showed that treatment of bystander cells with anti-TNFα monoclonal antibody (mAb) partially suppressed the nuclear factor-κB (NF-κB) and MAPK pathways. The observations that extracellularly applied antioxidant enzymes, such as superoxide dismutase (15) and catalase (16), can inhibit medium-mediated bystander response suggest a role of reactive radical species in the bystander process. Because mitochondria are the main source of energy production, as well as generators of free radicals in cells, especially in pathologic and stressful conditions, the present studies were conducted to define the contribution of mitochondria to the bystander response using mutagenesis as an end point. There is recent evidence that point mutations in the mitochondrial genome are induced among either directly irradiated cells with a 5-Gy dose of γ-rays or by exposure to bystander factor(s) obtained from such cells (17). To better understand the role of mitochondria in the radiation-induced bystander effect, mitochondrial DNA–depleted human skin fibroblasts (HSF; ρ^o) and their parental mitochondrial functional cells (ρ^+) were used in conjunction with the Columbia University charged particle microbeam and track segment irradiation system. Because TNFα and ROS may induce the inhibitor NF-κB kinase (IKK)–NF-κB pathways, we further examined the link between the NF-κB signaling pathway and the bystander response. In the present study, we found that ρ^o cells were more sensitive to α-particle induced bystander mutagenesis. In addition, NF-κB activity and both NF-κB–dependent COX-2 and inducible NO synthase (iNOS) expression levels were lower in bystander ρ^o cells compared with bystander ρ^+ cells. Furthermore, we found that Bay 11-7082, a pharmacologic inhibitor of NF-κB activation, and 2-(4-carboxyphenyl)-4,4,5,5-tetramethylimidazoline-1-oxyl-3-oxide (c-PTIO), a scavenger of NO, significantly decreased the mutation frequency in both bystander ρ^o and ρ^+ cells. Our results indicated that mitochondria played an important role in radiation-induced bystander effect, partially via mitochondria-dependent regulation of iNOS and COX2 signaling pathways.

Materials and Methods

Cell culture. ρ^o cells were generated by treatment of parental (ρ^+) HSFs with 50 ng/mL ethidium bromide in growth medium supplemented with 50 μg/mL uridine, as described before (18). The ρ^+ cells were maintained in a 4.5 g/L glucose DMEM with 4 mmol/L L-glutamine and 110 mg/L sodium pyruvate supplemented with 10% fetal bovine serum, 100 IU/mL penicillin, and 100 μg/mL streptomycin. The ρ^o cells were cultured using the same medium plus 50 μg/mL uridine (Sigma), which provides an alternative

Requests for reprints: Tom K. Hei, Center for Radiological Research, Columbia University Medical Center, 168 West 168th Street, VC 11-204, New York, NY 10032. Phone: 212-305-8462; Fax: 212-305-3229; E-mail: tkh1@columbia.edu.

doi:10.1158/0008-5472.CAN-07-5278

source of energy through glycolysis to ensure optimal growth (19). Primary normal human lung fibroblasts (NHLF) in frozen vials were purchased from Cambrex/Lonza. The NHLF cells were thawed and maintained in a fibroblast growth medium supplied by the manufacturer (14). Cultures were maintained at 37°C in a humidified 5% CO_2 incubator. The medium was changed every 3 d, and the cells were passaged at confluence.

Microbeam irradiation. Cell tracker orange (CTO, 1 μmol/L)–stained cells were mixed with nonstained, either same or different type cells, in a 1:10 ratio. Approximately, 3,000 exponentially growing mixed cells in a 1.5-μL volume were inoculated into each of a series of microbeam dishes coated with Cel-Tak (BD Biosciences) to enhance cell attachment as described (20, 21). The next day after plating, ~90% of the attached cells were in contact with neighboring cells. The image analysis system then located the centroid of each CTO-stained cells and irradiated all of them, one at a time, with an exact number of α-particles (90 keV/μm ^{3}He ions) accelerated with a 5-MV Singletron accelerator at the Radiological Research Accelerator Facilities of Columbia University. After irradiation, cells were maintained in the dishes overnight before being removed by trypsinization and replated into culture flasks for the mutant assay as described (20, 21). After previously described protocol, all controls were similarly stained and sham-irradiated as well.

Track segment irradiation procedure. The newly designed strip mylar dishes were used in the present studies as described (14, 22). Exponentially growing ρ^o and ρ^+ cells were plated in the concentric strip mylar dishes a couple of days before irradiation to ensure a confluent state. A 50-cGy dose of ^{4}He ions (120 keV/μm) was delivered to the cells as described above. After irradiation, at selected time points, the inner and outer mylar dishes were separated, and the cells from each growth surface were trypsinized and individually pooled for end point analysis.

Survival of irradiated and nonirradiated bystander cells. Nonirradiated bystander, irradiated, and control cells were collected after irradiation at different time points. Cultures were trypsinized and counted with a Coulter counter, and aliquots of the cells were replated into 100-mm-diameter dishes for colony formation. Representative aliquots of cells were further incubated for mutagenesis and other testings. Cultures for clonogenic survival assays were incubated for 12 d, at which time they were fixed with formaldehyde and stained with Giemsa. The number of colonies was counted to determine the surviving fraction as described (20, 21).

Cell proliferation. Aliquots of 1×10^5 ρ^o and ρ^+ cells were plated in T25 flasks. On days 1, 2, 4, 6, 8, 10, and 12 after plating, two flasks of cells were trypsinized and then counted with a Coulter counter. The average number of cells was plotted as a cell growth curve, and the doubling time of cells was calculated as described (23).

PCR analysis of mitochondrial DNA. Two different pairs of primers were chosen for mitochondrial DNA detection [primer 1 (251 bp) 1685–1709 (sense), 1912–1936 (antisense); primer 2 (261 bp) 3304–3324 (sense), 3543–3565 (antisense)]. PCR amplifications were performed for 30 cycles using a DNA thermal cycle model 9700 (Perkin-Elmer) in 50-μL reaction mixtures containing 0.5 μg of the DNA sample. Each PCR cycle consisted of denaturation at 95°C for 30 s, annealing at 55°C for 30 s, and extension at 72°C for 30 s. After the last cycle, samples were incubated at 72°C for an additional 10 min, electrophoresed on 1% agarose gels, and stained with ethidium bromide.

Oxygen consumption. Oxygen consumption in intact cells was assayed, as described previously (19). Briefly, 1×10^7 wild-type and ρ^o cells were suspended in 1.5 mL DMEM lacking glucose, and oxygen concentration was assayed over 3 min at 37°C in a Hansatech (MA) Clark's oxygen electrode unit.

Cellular staining with fluorescent probes and flow cytometry. Cells were stained with fluorescent dyes diluted in DMEM. The following dye combinations were added for 45 min at 37°C in the dark (*a*) 20 nmol/L dihexyloxacarbocyanine iodide (DiOC6 for assessment of mitochondrial membrane potential, Δψm; Invitrogen), (*b*) 2 μmol/L hydroethidine (HE for assessment of superoxide production; Invitrogen), and (*c*) 3.5 μmol/L 4-amino-5-methylamino-2OE,7OE-difluorofluorescein diacetate (DAF-FM for the detecting of NO; Invitrogen). Flow cytometry was performed using a FACSCalibur (Becton Dickinson) to analyze fluorescent signaling, propidium iodide staining of DNA and cell cycle distribution. DiOC6 and DAF-FM fluorescence were analyzed in the FL1 channel, whereas HE fluorescence was analyzed using the FL3 channel. Forward and side scatter data were used to gate out cellular fragments.

Quantification of mutations at the *hypoxanthine phosphoribosyltransferase* locus. To determine the hypoxanthine phosphoribosyltransferase$^-$ (HPRT$^-$) mutant fraction, after a 7-d expression period, 2×10^5 cells per dish were plated into 25 to 30 dishes (100 mm) in a total of

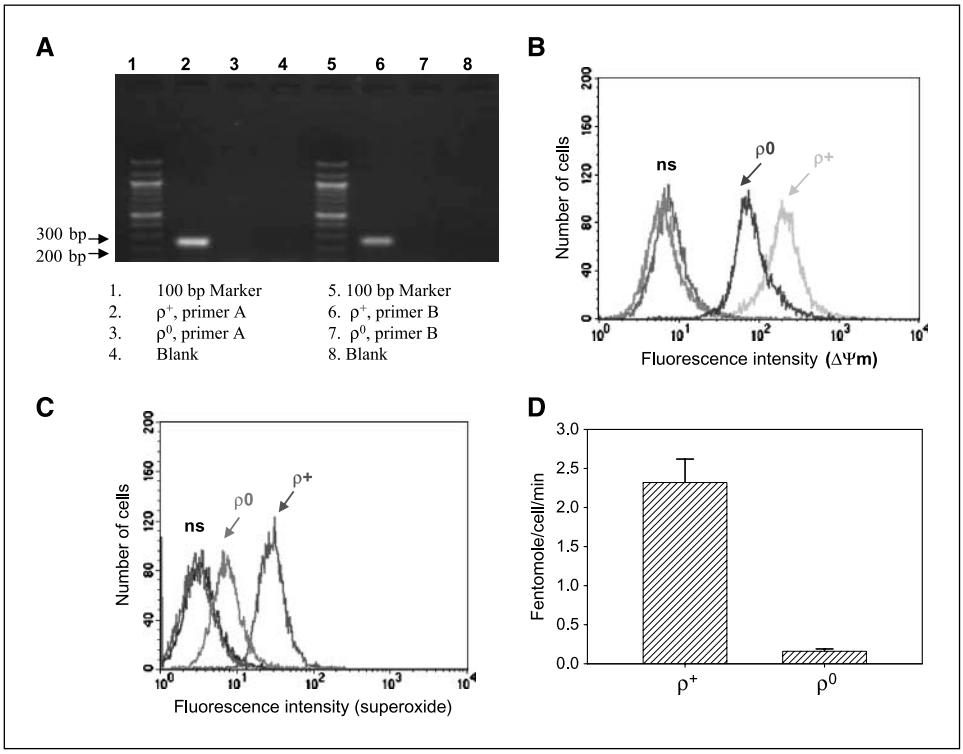

Figure 1. Characterization of mitochondrial DNA–depleted HSFs (ρ^o) and their parental cells (ρ^+). *A,* PCR amplification of genomic DNA from ρ^o and ρ^+ cells using two different segments of mitochondrial DNA as primers. PCR products for the two primer sets: primer A (251 bp) and primer B (261 bp). *B,* assessment of mitochondrial membrane potential (Δψm) in ρ^+ and ρ^o cells using DiOC6 staining (20 nmol/L) and flow cytometry. ρ^o cells show lower membrane potential compared with ρ^+ cells. *C,* assessment of superoxide production in ρ^o and ρ^+ cells using HE (2 μmol/L) and flow cytometry. ρ^o cells show lower superoxide production compared with ρ^+ cells. *D,* rates of oxygen consumption for ρ^+ and ρ^o cells using an oxygen electrode unit. Average of duplicate determinants from two or three independent clones from each line; *bars,* SD.

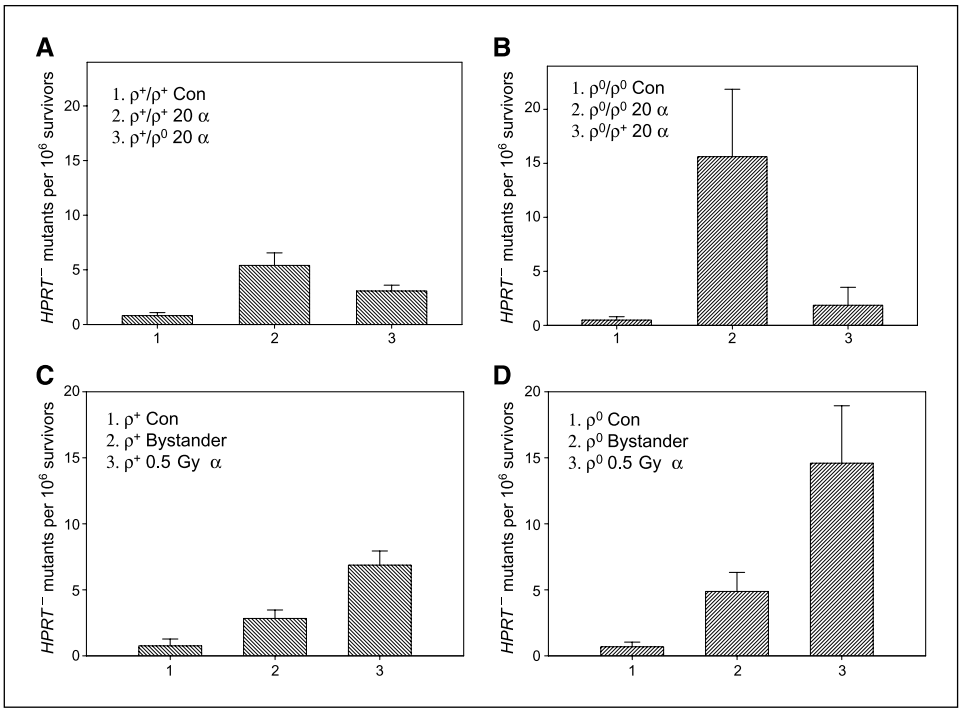

Figure 2. *HPRT*$^-$ mutation of bystander cells in mixed cultures of ρ^+ and ρ^o cells using the Columbia microbeam. *A,* ρ^+ cells were used as the bystander cells when 10% of ρ^o or ρ^+ cells were irradiated with 20 α-particles each. *B,* ρ^o cells were used as the bystander cells when 10% of ρ^+ or ρ^o cells were irradiated with 20 α-particles each. *C, HPRT*$^-$ mutation of bystander and directly irradiated ρ^+ cells exposed to a 0.5-Gy dose of α-particles using the specially designed strip dishes. *D,* same as *C* but with ρ^o cells. *Columns,* data pooled from three to five independent experiments; *bars,* SD.

12 mL of the growth medium, containing 100 μmol/L 6-thioguanine (Sigma Chemical). The cultures were further incubated for 12 d, at which time, the cells were fixed and stained, and the number of *HPRT*$^-$ mutant colonies scored. Meanwhile, aliquots of 250 cells were plated in dishes containing growth medium without 6-thioguanine for determination of plating efficiency. The mutant fraction was calculated as the number of surviving colonies divided by the total number of cells plated after correction for plating efficiency.

Micronuclei scoring. The cytokinesis block technique was used for the micronuclei assay. Briefly, cultures were treated with 1 μg/mL cytochalasin-B for 32 h and then fixed with 4% paraformaldehide for 20 min. Air-dried cells were covered/stained with DAPI mounting solution. Micronuclei were scored in the binucleated cells and classified according to standard criteria (24). The micronuclei yield was calculated as the ratio of number of micronuclei to the scored number of binucleated cells.

Western blotting. Protein was extracted from either the control or bystander cells by lysis in extracting buffer [50 mmol/L Tris-HCl (pH 8). 150 mmol/L NaCl, 1% NP40, 0.1% SDS, 1 mmol/L phenylmethylsulfonyl fluoride, and a mixture of protease inhibitors (Roche)]. The concentration of the protein was determined by the Bio-Rad Protein Assay (Bio-Rad). Equivalent amounts of protein (50–100 μg) were fractionated on a 10% SDS-polyacrylamide gel for 3 h, and proteins were transferred to nitrocellulose membranes under semidry conditions. Mouse monoclonal anti-human COX-2 (Cayman), mouse polyclonal antibody against iNOS (Cell Signaling), and mAb against β-actin (Sigma) were used. The secondary antibodies were horseradish peroxidase–conjugated antimouse or antirabbit IgG diluted 1:5,000 to 1:10,000. After electrochemiluminescence, the band intensities were evaluated by phosphorimaging and normalized to β-actin protein level.

Electrophoretic mobility shift assay. The electrophoretic mobility shift assay (EMSA) was performed for the detection of NF-κB DNA-binding activity, as previously described using the labeled double-strand oligonucleotide AGCTT*GGGGACTTTCC*AGGCG (binding site is italicized). Ubiquitous NF-Y DNA-binding activity was used as an internal control (25).

Statistical analysis. Data were calculated as means and SDs. Comparisons of surviving fractions and induced mutant fractions between treated and control groups were made by the Students' *t* tests. A *P* value of 0.05 or less between groups was considered significant.

Results

Characterization of mitochondrial DNA–depleted (ρ^o) cells and their parental (ρ^+) cells. A series of experiments were conducted to characterize the differences between ρ^o cells and their parental ρ^+ cells. In the presence of uridine, ρ^o cells grew very well in culture. Addition of uridine to culture medium did not affect the radiosensitivity of HSF and the dose-response survival curves of ρ^o and ρ^+ HSF culture were similar (data not shown). Compared with ρ^+ cells, ρ^o cells showed only a slight decrease in saturation density as the culture approached confluency (data not shown). Using two different primer sets that corresponded to different segments of the mitochondrial DNA, we detected no mitochondrial DNA band in ρ^o cells; in contrast, a clear band was detected in ρ^+ cells with either of the primer pairs (Fig. 1*A*). When the cells were stained with the mitochondrial membrane potential probe DiOC6, ρ^o cells showed a decrease in fluorescence intensity (mean intensity, 95.1 arbitrary units, A.U.) relative to control ρ^+ cells (mean intensity, 226 A.U.; Fig. 1*B*). Likewise, mitochondrial DNA–depleted cells showed a decrease in intracellular superoxide content (mean intensity, 8.2 A.U.) when compared with wild-type cells (mean intensity, 30.0 A.U.; Fig. 1*C*). To further confirm that ρ^o cells had compromised mitochondrial function, we showed that these cells had an oxygen consumption level that was 20 times less than wild-type cells (Fig. 1*D*). These data clearly indicate that ρ^o cells have dysfunctional mitochondria and that this cell line is a good model to investigate the role of mitochondria in radiation-induced bystander responses.

α-Irradiation induces a higher bystander mutagenic rate in ρ^o cells than in ρ^+ cells. To explore the role of mitochondria in the radiation-induced bystander effect, a microbeam was used to lethally irradiate either ρ^o or ρ^+ cells with 20 α-particles, each in a mixed confluent culture, and the bystander response was determined in the nonirradiated fraction. We found that ρ^o cells, when compared with ρ^+ cells, showed a higher bystander *HPRT*$^-$

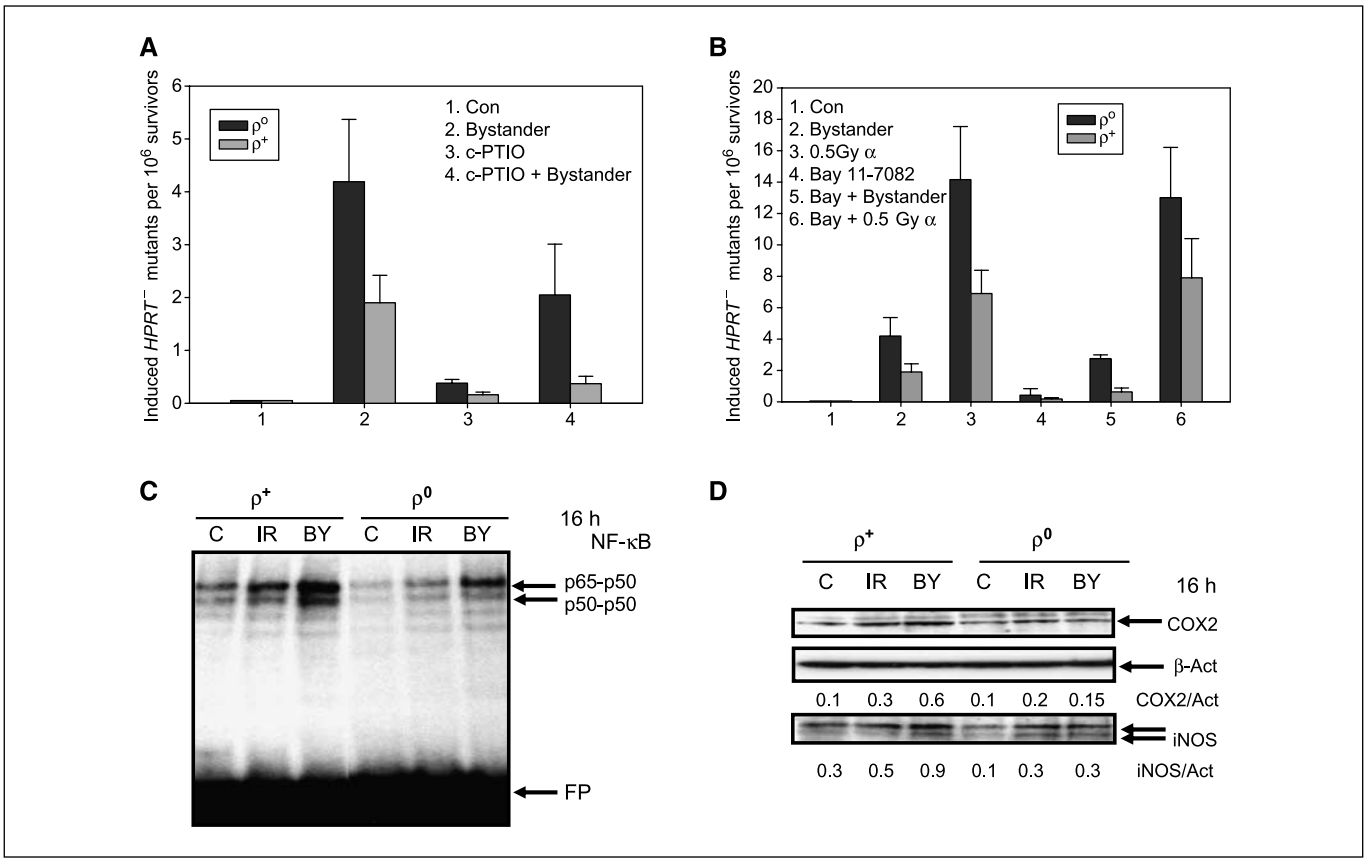

Figure 3. *A,* effect of the NO scavenger c-PTIO (20 μmol/L, 2 h before and maintained overnight after irradiation) on *HPRT*⁻ mutant fractions of ρ^+ and ρ^o cells. *B,* effect of the NF-κB inhibitor Bay 11-7082 (1 μmol/L, 2 h before and maintained overnight after irradiation) on *HPRT*⁻ mutant fractions of ρ^+ and ρ^o cells. Data are from three to four independent experiments; *bars,* SD. *C,* characterization of NF-κB DNA-binding activities of control, bystander cells, and directly irradiated (0.5 Gy dose of α-particles) ρ^+ and ρ^o cells using EMSA. *FP,* free-labeled oligonucleotide probe. *D,* Western blot analysis of COX-2 and iNOS protein levels in bystander and directly irradiated (0.5 Gy dose of α-particles) ρ^+ and ρ^o cells. β-Actin was used as loading control.

mutagenic response (15.2 versus 5.4 per 10^6 survivors, $P < 0.05$) in confluent monolayer when 10% of the same population were lethally irradiated (Fig. 2*A* and *B*). It should be noted that the background mutant fraction of ρ^o and ρ^+ cells was similar being ~1.0 per 10^6 survivors. However, using mixed cultures of ρ^o and ρ^+ cells and targeting only one population of cells with a lethal dose of α-particles, a decreased bystander mutagenesis was uniformly found with both cell types. For example, when 10% of the CTO-stained ρ^o cells (in culture with 90% of nonstained ρ^o cells) were irradiated with 20 α-particles, the mutant fraction among the nonhit bystander ρ^o cells was ~15.2 per 10^6 survivors. However, when a similar number of ρ^o cells were irradiated among 90% of wild-type cells, the resultant bystander mutant fraction was only 3.1 per 10^6 surviving ρ^+ cells ($P < 0.05$). Similarly, when 10% CTO-stained ρ^+ cells were lethally irradiated with α-particles, the mutant yield was ~5.4 in 10^6 surviving bystander ρ^+ cells, but only 1.8 per 10^6 surviving bystander ρ^o cells ($P < 0.05$). These results indicate that mitochondria-deficient cells cannot effectively communicate the bystander signals with wild-type cells; or alternatively, signals from one cell type can modulate expression of bystander response in another cell type.

Track segment irradiation confirms bystander mutagenesis in ρ^o and ρ^+ cells. Because the microbeam can only irradiate a limited number of cells, to generate sufficient bystander cells for mechanistic studies, we used the specially designed strip mylar dishes and track segment irradiation as described (14, 21). Because cells that were seeded on the thicker mylar (38 μm) would not be traversed by α-particles but would be in the vicinity of those seeded on thinner mylar (6 μm) that would, we had, effectively, a pure population of bystander cells. Exposure of ρ^+ cells to a dose of 0.5 Gy α-particles increased the bystander *HPRT*⁻ mutant yield to a level 2.6 times higher than the background incidence. However, under similar irradiation conditions, ρ^o cells had a bystander mutant fraction that was 7.1-fold higher than nonirradiated ρ^o cells (Fig. 2*C* and *D*). These results are consistent with the data generated from microbeam irradiation, showing that mitochondria-deficient cells have a higher mutation frequency in both directly irradiated and bystander cells. Comparing with the data generated using the microbeam, the bystander mutagenesis obtained using the broad, track segment beam for both the ρ^+ and ρ^o HSFs was significantly reduced ($P < 0.05$).

Effect of c-PTIO on bystander mutagenesis. To determine if NO is linked to mitochondrial function in mediating the bystander response, we treated cells with 20 μmol/L c-PTIO, a NO scavenger, 2 hours before and maintained overnight after irradiation. As shown in Fig. 3*A*, treatment with c-PTIO significantly reduced the bystander mutagenesis in both ρ^o and ρ^+ cell lines ($P < 0.05$). However, the effect of c-PTIO on the bystander response in ρ^+ cells was more pronounced than in ρ^o cells. The induced mutation frequency was reduced from 1.90 to 0.37 per 10^6 survivors (5.1-fold)

in wild-type cells compared with a reduction from 4.19 to 2.05 per 10^6 survivors (2.0-fold) in ρ^o cells. These results indicated that, in addition to NO, other signaling molecules might play a role in modulating the bystander effects in mitochondria-deficient cells.

Role of NF-κB in the bystander response. Expression of the iNOS gene is controlled by the transcription factor NF-κB. To define the function of NF-κB in radiation-induced bystander effects, cells were treated with 1 μmol/L Bay 11-7082, a pharmacologic inhibitor of IKK–NF-κB activation, 2 hours before irradiation, and maintained overnight after irradiation. The dose of Bay 11-7082 used was nontoxic, nonmutagenic in both ρ^o and ρ^+ cell lines. Treatment of both cell types with Bay 11-7082 resulted in a significant reduction of the bystander mutagenesis ($P < 0.05$; Fig. 3*B*). The inhibition by Bay 11-7082 on radiation-induced bystander effects was similar to that of c-PTIO: being more effective in ρ^+ (3.0-fold, $P < 0.01$) than in ρ^o cells (1.5-fold, $P < 0.05$). Consistent with these observations, we found that the basal and inducible (both directly irradiated and bystander) levels of nuclear NF-κB DNA-binding activity were notably higher in ρ^+ compared with ρ^o cells (Fig. 3*C*). Consequently, expression levels of NF-κB–dependent proteins, such as iNOS and COX-2, were notably lower in ρ^o cells (Fig. 3*D*).

We previously reported that the COX-2/prostaglandin E2 (PGE2) signaling pathway, which is a hallmark of inflammation and ROS production, was critically linked to radiation bystander phenomenon in normal human fibroblasts (14). In the present study, 3-fold and 6-fold increases in COX-2 expression level were found in directly irradiated and bystander ρ^+ cells, respectively (Fig. 3*D*). However, COX-2 expression increased only slightly in directly irradiated and bystander ρ^o cells (Fig. 3*D*). Taken together, these results indicated that inducible (but not basal) expression of COX-2, which was substantially lower in mitochondria-deficient cells, plays a critical role in regulating mechanisms of bystander effects, which is consistent with our previous findings (14). However, these results also pointed out that other mechanisms of radiation-induced bystander effect might be different in mitochondria-deficient cells. Furthermore, we cannot exclude that signaling pathways, other than the COX-2/PGE2 and iNOS/NO pathways, might be activated by NF-κB and can induce bystander mutagenesis.

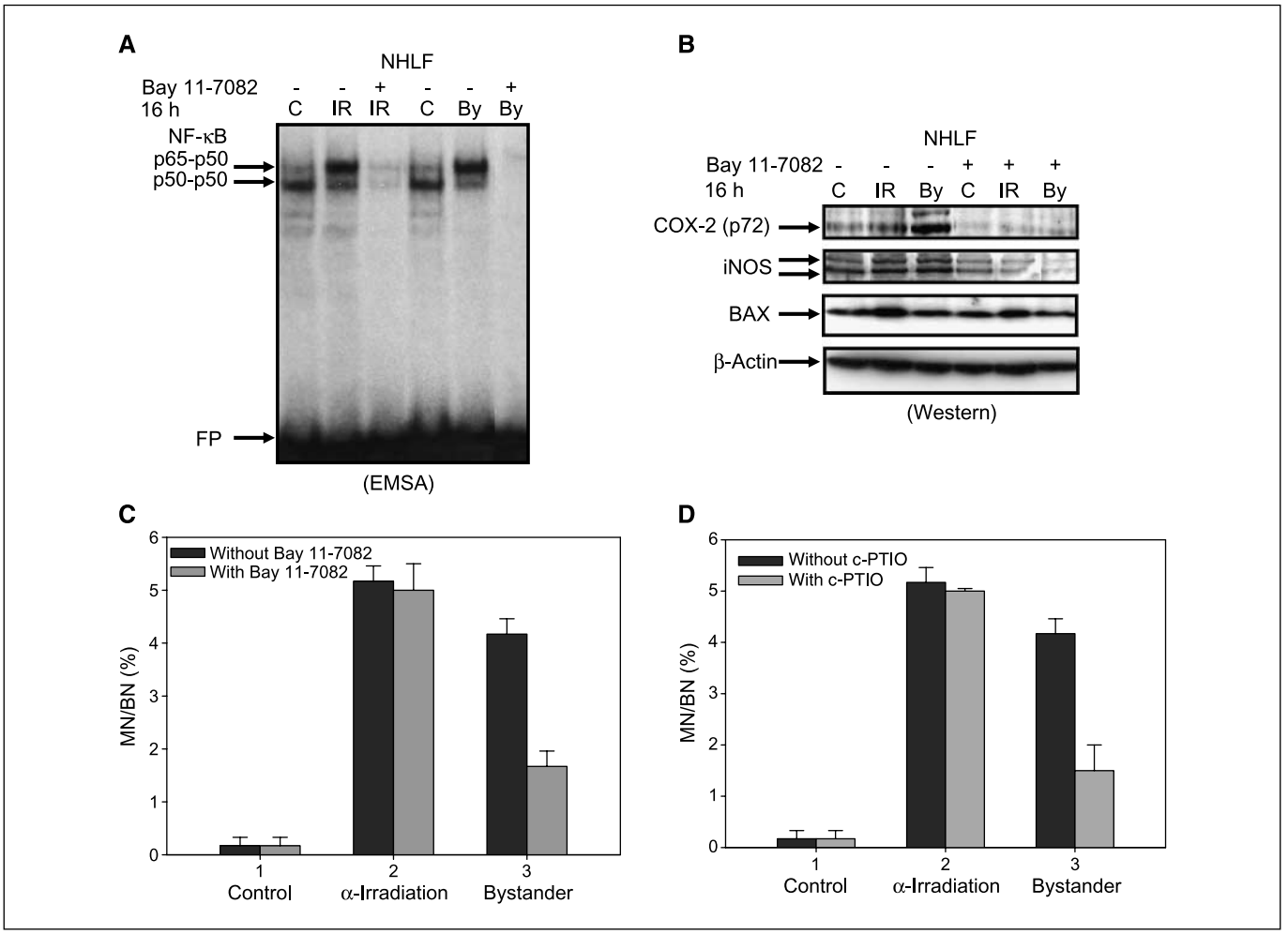

Figure 4. Effects of NF-κB inhibition on NF-κB–dependent COX-2 and iNOS protein levels, and micronuclei formation in bystander and directly irradiated NHLFs. Cells were treated with 0.5 Gy α-particles in specially designed strip dishes with or without Bay 11-7082 (1 μmol/L). *A,* EMSA was performed with nuclear extracts of directly irradiated and bystander NHLF 16 h after irradiation. Two NF-κB DNA-binding complexes, p65-p50 and p50-p50, are indicated. *B,* Western blot analysis of COX-2, iNOS, BAX, and β-actin levels in NHLF after indicated treatment. *C* and *D,* effect of Bay 11-7082 and c-PTIO (1 and 20 μmol/L, respectively) on micronuclei formation in irradiated and bystander cells. Data are pooled from three independent experiments; *bars,* SD.

Role of NF-κB in α-particle–induced bystander effects in NHLF. Because NF-κB is an important transcription factor for many signaling genes, including COX-2, we used NHLF cultures, which were used previously to document COX-2 activities in bystander signaling (14), to examine the role of NF-κB in the bystander response. α-Particle irradiation up-regulated NF-κB–binding activity in both directly irradiated and bystander cells, whereas Bay 11-7082, a pharmacologic inhibitor of the IKK/NF-κB, efficiently suppressed this up-regulation and also reduced levels below basal amount (Fig. 4*A*). This inhibitor of NF-κB activity also efficiently down-regulated COX-2 and iNOS expression levels in both directly irradiated and bystander fibroblasts (Fig. 4*B*). Micronuclei formation was readily detected in directly irradiated and bystander cells, whereas both Bay 11-7082 (Fig. 4*C*) and c-PTIO (Fig. 4*D*) effectively decreased this level in bystander cells ($P < 0.05$).

Effects of cytokines on the bystander effects. TNFα might be an excellent candidate in mediating bystander effects in NHLF. Exogenous TNFα in concert with IL1β directly controls COX-2 expression in NHLF (Fig. 5*A*). Both TNFα and IL1β could be induced after α-irradiation of NHLF. The inhibitory mAb against TNFα, which was introduced into the cell media, substantially decreased levels of NF-κB (Fig. 5*B*) and c-Jun-NH_2-kinase (JNK; data not shown) that was accompanied by a well-pronounced decrease in the COX-2 expression level in both irradiated and, especially, in bystander NHLF (Fig. 5*C*). Simultaneously, the negative effect of anti-TNF mAb on extracellular signal-regulated kinase (ERK) activity (phosphorylated ERK protein level) was relatively modest (data not shown). As an additional physiologic test, we determined clonogenic survival of NHLF during a partial suppression of TNF levels by the inhibitory effect of anti-TNF mAb. We found a significant increase in cell survival of bystander cells treated with anti-TNF mAb ($P < 0.05$; Fig. 5*D*).

Discussion

Although radiation-induced bystander effects have attracted much attention in the past decade, the mechanisms of the process remain unclear. It is likely that cellular signaling pathways, for example, membrane ligands and the downstream MAPK cascade, provide a common link between medium-mediated and gap-junction–dependent bystander phenomena. Previous studies by Mitchell et al. have shown that when 10% of cells are exposed to α-particles, a significantly greater number of cells are inactivated when irradiated at high density (>90% in contact with neighbors) than at low density (<10% in contact). In addition, the bystander oncogenic transformation frequency is significantly higher in high-density cultures (26). These results suggest that when cells are traversed by α-particles, the transmission of a bystander signal through cell-to-cell contact results in a higher response compared with those mediated by soluble factors. In the present study, we observed a similar density-dependent bystander response. In microbeam irradiation, a higher bystander mutagenesis was found because cells had more cell-cell contact compared with cells plated in specially designed strip dishes.

Nitric oxide has been postulated to be a potential signaling molecule in radiation-induced bystander effects (27–29). Shao et al. reported that when only 1% of cell nuclei were individually targeted

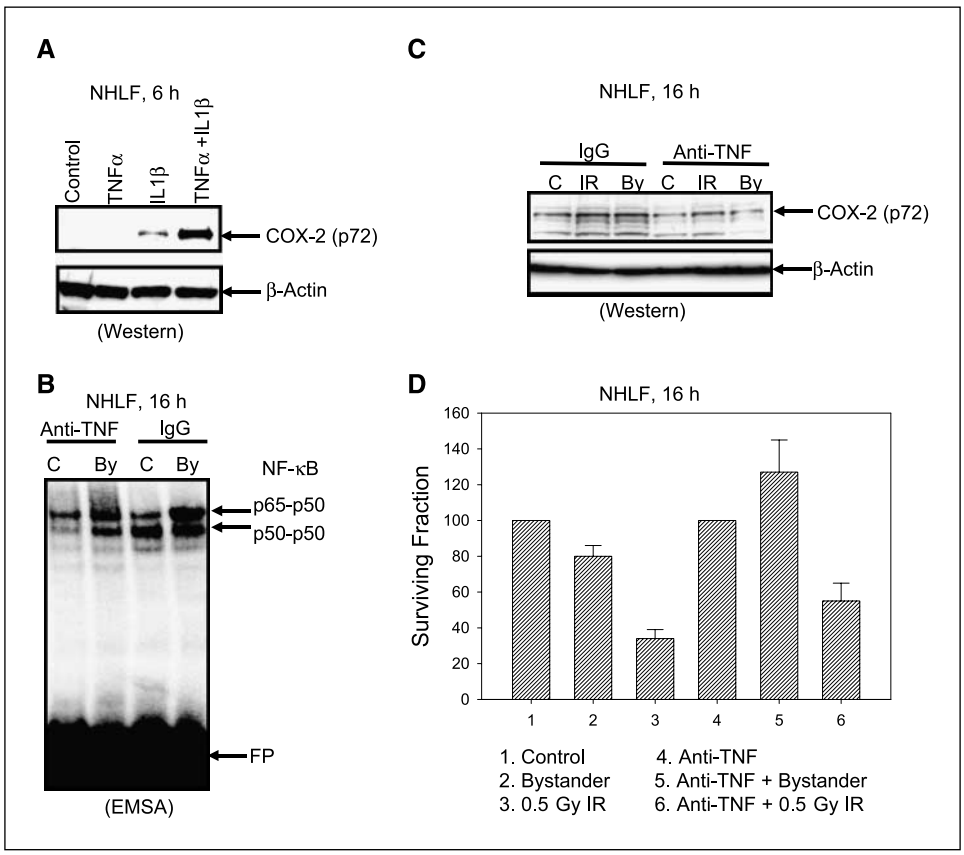

Figure 5. Effects of TNFα on the bystander effects. *A,* combined treatment of NHLF with TNFα (20 ng/mL) and IL1β (2 ng/mL) induced COX-2 expression as determined by Western blot analysis. *B,* EMSA of NF-κB DNA-binding activity in control and bystander cells, with or without anti-TNF mAb (5 μg/mL) in the medium. *C,* effects of treatment with the inhibitory anti-TNF mAb (5 μg/mL) on COX-2 levels in control, α-irradiated, and bystander cells. *D,* clonogenic survival assay of NHLF after indicated treatment with and without inhibitory anti-TNF mAb (5 μg/mL). Data are pooled from three independent experiments; *bars,* SD.

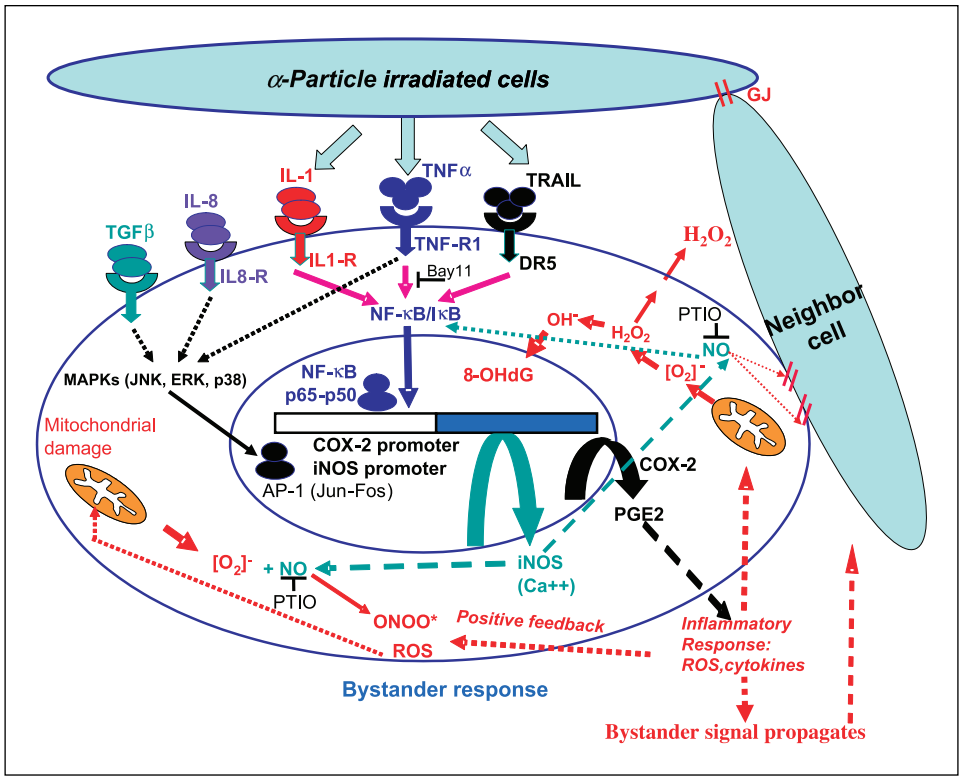

Figure 6. A unifying model of the signaling pathways involved in radiation-induced bystander effects. Secreted or membrane forms of cytokines, such as TNFα, activate IKK-mediated phosphorylation of IκB, which releases NF-κB, that enters the nucleus and acts as a transcription factor for *COX-2* and *iNOS*. TNFα also activates MAPK pathways (ERK, JNK, and p38) that via activator protein 1 transcription factor additionally up-regulate expression of *COX-2* (14) and iNOS, which stimulate the production of NO. Mitochondrial damage facilitates the production of hydrogen peroxide that migrates freely across plasma membrane and is subjected to antioxidant removal. Activation of COX-2 provides a continuous supply of reactive radicals and cytokines for the propagation of the bystander signals either through gap junction or medium.

with a single helium ion, ~40% of the cells showed an increase in fluorescence intensity of the NO-sensitive dye, DAF-FM. Moreover, it was found that when only one cell in a population of ~1,200 cells was targeted with one or five ions, the incidence of micronuclei increased by 20% and concurrent treatment with c-PTIO significantly reduced the bystander effect (30). In the present study, we found that the NO scavenger had a similar suppressive effect on bystander mutagenesis of both ρ^+ and ρ^o cells, although the effects were more pronounced in the former. Because mitochondria are the main source of reactive radical species in cells, the basal level of free radicals in ρ^o cells is lower than in mitochondrial functional cells (Fig. 1*B–D*). There is evidence that, in ρ^o cells with a complete shutdown of the electron transport chain, the decreased level of reactive oxygen species resulted in a down-regulation of the manganese superoxide dismutase, glutathione, and glutathione peroxidase, an important intracellular antioxidant pool (31). As such, compared with wild-type cells, ρ^o cells are more susceptible to oxidative stress and expressed in a higher bystander mutagenesis as shown in the present studies. It is likely that one or more other signaling molecules, in addition to NO, are involved in radiation induced bystander effects in mitochondria-deficient cells. This could explain the difference in bystander signaling response in mixed cultures of ρ^+ and ρ^o cells. Alternatively, ρ^o cells, by virtue of their reduced apoptotic response,[4] may accumulate a higher mutant fraction. This will be consistent with the higher bystander response seen in these cells. It is also possible that signal from one cell line can modulate expression of bystander response in another cell type (32) and is consistent with the findings with the mixed cell population (Fig. 2*A* and *B*).

Elevated levels of NO have been detected in a variety of pathophysiologic processes, including inflammation and carcinogenesis (33, 34). In our previous study, we found that COX-2 is critically linked to the radiation-induced bystander effect in normal human fibroblasts (14). There is evidence that NO can induce expression of COX-2 in mouse skin and human cultured airway epithelial cells and that the NF-κB pathway is involved in the process (35, 36). Our findings that Bay 11-7082, a specific IKK/NF-κB inhibitor, could eliminate bystander mutagenesis in both wild-type and ρ^o cells highlight the important role of this transcription factor in the bystander phenomenon (Fig. 3*B*). NF-κB directly controls gene expression of COX-2 and iNOS. As proposed in our working model, cytokines of the TNFα superfamily might be excellent candidates in mediating bystander effects (Fig. 6). Ionizing radiation is a strong inducer of the ATM-IKK-NF-κB signaling pathway (37), which is further involved in the up-regulation of TNFα gene expression (38). Secreted or membrane forms of TNFα could induce bystander effects in nonirradiated cells via activation of COX-2 gene expression, as we observed in the present study. Inhibitory mAb against TNF partially suppressed NF-κB activation and the subsequent COX-2 up-regulation in both directly irradiated and bystander cells (Fig. 5). Taken together, our data showed a connection between up-regulation of NF-κB activation and mitochondrial function in mediating the bystander phenomenon. Indeed, NF-κB–dependent functions are characteristic for both ρ^+ and ρ^o cells, although in the last case, levels of inducible NF-κB activity were substantially lower (Fig. 3*C*). As expected, in cells with functional mitochondria, up-regulation of COX-2 was detected in both directly irradiated and bystander cells (Fig. 3*D*). This increase in COX-2 expression levels was almost

[4] V.N. Ivanov and T.K. Hei, unpublished observation.

completely blocked in the presence of Bay 11-7082 (Fig. 4*B*). It indicates that the NF-κB/COX-2/PGE2 and NF-κB/iNOS/NO pathways are critical to the radiation induced bystander effect in mitochondrial functional cells. However, in ρ^0 cells, the contribution of COX-2 to the bystander process is less pronounced, whereas NF-κB/iNOS/NO pathway actively operates, although at lower level compared with normal cells.

Acknowledgments

Received 9/12/2007; revised 11/7/2007; accepted 12/27/2007.

Grant support: NIH grants CA 49062 and ES 12888 and National Cancer Institute Research Resource grant 11623.

The costs of publication of this article were defrayed in part by the payment of page charges. This article must therefore be hereby marked *advertisement* in accordance with 18 U.S.C. Section 1734 solely to indicate this fact.

We thank Dr. Howard Lieberman for critical reading of the manuscript.

References

1. Morgan WF. Non-targeted and delayed effects of exposure to ionizing radiation: I. Radiation-induced genomic instability and bystander effects *in vitro*. Radiat Res 2003;159:567–80.
2. Morgan WF. Non-targeted and delayed effects of exposure to ionizing radiation: II. Radiation-induced genomic instability and bystander effects *in vivo*, clastogenic factors and transgenerational effects. Radiat Res 2003;159:581–96.
3. Hei TK, Persaud R, Zhou H, Suzuki M. Genotoxicity in the eyes of bystander cells. Mutat Res 2004;568:111–20.
4. Mothersill C, Seymour CB. Radiation-induced bystander effects-implications for cancer. Nat Rev Cancer 2004; 4:158–64.
5. Hickman AW, Jaramillo RJ, Lechner JF, Johnson NF. α-particle-induced p53 protein expression in a rat lung epithelial cell strain. Cancer Res 1994;54:5797–800.
6. Deshpande A, Goodwin EH, Bailey SM, Marrone BL, Lehnert BE. α-particle-induced sister chromatid exchange in normal human lung fibroblasts: evidence for an extranuclear target. Radiat Res 1996;145:260–7.
7. Narayanan PK, Goodwin EH, Lehnert BE. α Particles initiate biological production of superoxide anions and hydrogen peroxide in human cells. Cancer Res 1997;57: 3963–71.
8. Mothersill C, Seymour CB. Cell-cell contact during γ irradiation is not required to induce a bystander effect in normal human keratinocytes: evidence for release during irradiation of a signal controlling survival into the medium. Radiat Res 1998;149:256–62.
9. Iyer R, Lehnert BE. Factors underlying the cell growth-related bystander responses to α particles. Cancer Res 2000;60:1290–8.
10. Azzam EI, de Toledo SM, Gooding T, Little JB. Intercellular communication is involved in the bystander regulation of gene expression in human cells exposed to very low fluencies of α particles. Radiat Res 1998;150: 497–504.
11. Azzam EI, de Toledo SM, Little JB. Direct evidence for the participation of gap junction-mediated intercellular communication in the transmission of damage signals from α-particle irradiated to nonirradiated cells. Proc Natl Acad Sci U S A 2001;98:473–8.
12. Zhou H, Randers-Pehrson G, Waldren CA, Vannais D, Hall EJ, Hei TK. Induction of a bystander mutagenic effect of α particles in mammalian cells. Proc Natl Acad Sci U S A 2000;97:2099–104.
13. Zhou H, Suzuki M, Randers-Pehrson G, et al. Radiation risk to low fluences of α particles may be greater than we thought. Proc Natl Acad Sci U S A 2001; 98:14410–5.
14. Zhou H, Ivanov VN, Gillespie J, et al. Mechanism of radiation-induced bystander effect: role of the cyclooxygenase-2 signaling pathway. Proc Natl Acad Sci U S A 2005;102:14641–6.
15. Yang H, Asaad N, Held KD. Medium-mediated intercellular communication is involved in bystander responses of X-ray-irradiated normal human fibroblasts. Oncogene 2005;24:2096–103.
16. Lyng FM, Maguire P, McClean B, Seymour C, Mothersill C. The involvement of calcium and MAP kinase signaling pathways in the production of radiation-induced bystander effects. Radiat Res 2006; 165:400–9.
17. Murphy JE, Nugent S, Seymour C, Mothersill C. Mitochondrial DNA point mutations and a novel deletion induced by direct low-LET radiation and by medium from irradiated cells. Mutat Res 2005;585:127–36.
18. Liu SX, Davidson MM, Tang X, et al. Mitochondrial damage mediates genotoxicity of arsenic in mammalian cells. Cancer Res 2005;65:3236–42.
19. Partridge MA, Huang SX, Hernandez-Rosa E, Davidson MM, Hei TK. Arsenic induced mitochondrial DNA damage and altered mitochondrial oxidative function: implications for genotoxic mechanisms in mammalian cells. Cancer Res 2007;67:5239–47.
20. Hei TK, Wu LJ, Liu SX, Vannais D, Waldren CA. Mutagenic effects of a single and an exact number of α particles in mammalian cells. Proc Natl Acad Sci U S A 1997;94:3765–70.
21. Wu L, Randers-Pehrson G, Xu A, et al. Targeted cytoplasmic irradiation with α particles induces mutations in mammalian cells. Proc Natl Acad Sci U S A 1999; 96:4959–64.
22. Zhu A, Zhou H, Leloup C, et al. Differential impact of mouse Rad9 deletion on ionizing radiation-induced bystander effects. Radiat Res 2005;164:655–61.
23. Zhou H, Calaf G, Hei TK. Malignant Transformation of human bronchial epithelial cells with tobacco-specific nitrosamine, 4-methynitrosamine-1–3-pyridyl-1-butanone (NNK). Int J Cancer 2003;106:821–6.
24. Albertini RJ, Anderson D, Douglas GR, et al. IPCS guidelines for the monitoring of genotoxic effects of carcinogens in humans. International Programme on Chemical Safety. Mutat Res 2000;463:111–72.
25. Ivanov V, Fleming TJ, Malek TR. Regulation of nuclear factor-κ B and activator protein-1 activities after stimulation of T cells via glycosylphosphatidylinositol-anchored Ly-6A/E. J Immunol 1994;153:2394–406.
26. Mitchell SA, Randers-Pehrson G, Brenner DJ, Hall EJ. The bystander response in C3H 10T1/2 cells: the influence of cell-to-cell contact. Radiat Res 2004;161:397–401.
27. Sokolov MV, Smilenov LB, Hall EJ, Panyutin IG, Bonner WM, Sedelnikova OA. Ionizing radiation induces DNA double-strand breaks in bystander primary human fibroblasts. Oncogene 2005;24:7257–65.
28. Shao C, Folkard M, Michael BD, Prise KM. Targeted cytoplasmic irradiation induces bystander responses. Proc Natl Acad Sci U S A 2004;101:13495–500.
29. Müller WE, Ushijima H, Batel R, et al. Novel mechanism for the radiation-induced bystander effect: nitric oxide and ethylene determine the response in sponge cells. Mutat Res 2006;597:62–72.
30. Shao C, Stewart V, Folkard M, Michael BD, Prise KM. Nitric oxide-mediated signaling in the bystander response of individually targeted glioma cells. Cancer Res 2003;63:8437–42.
31. Isaac AO, Dukhande VV, Lai JC. Metabolic and antioxidant system alterations in an astrocytoma cell line challenged with mitochondrial DNA deletion. Neurochem Res. Epub 2007 Jun 12.
32. Mothersill C, Seymour C. Medium from irradiated human epithelial cells but not human fibroblasts reduces the clonogenic survival of unirradiated cells. Int J Radiat Biol 1997;71:421–7.
33. Czapski GA, Cakala M, Chalimoniuk M, Gajkowska B, Strosznajder JB. Role of nitric oxide in the brain during lipopolysaccharide-evoked systemic inflammation. J Neurosci Res. Epub 2007 Apr 26.
34. Seril DN, Liao J, Yang G-Y. Colorectal carcinoma development in inducible nitric oxide synthase-deficient mice with dextran sulfate sodium-induced ulcerative colitis. Mol Carcinog 2007;46:341–53.
35. Chun K-S, Cha H-H, Shin J-W, et al. Nitric oxide induces expression of cyclooxygenase-2 in mouse skin through activation of NF-κB. Carcinogenesis 2004;25: 445–54.
36. Watkins DN, Garlepp M, Thompson PJ. Regulation of the inducible cyclo-oxygenase pathway in human cultured airway epithelial (A549) cells by nitric oxide. Br J Pharmacol 1997;121:1482–8.
37. Hacker H, Karin M. Regulation and function of IKK and IKK-related kinases. Sci STKE 2006;357:re13.
38. Karin M. nuclear factor-κB in cancer development and progression. Nature 2006;441:431–6.

Mitochondrial Function and Nuclear Factor-κB–Mediated Signaling in Radiation-Induced Bystander Effects

Hongning Zhou, Vladimir N. Ivanov, Yu-Chin Lien, et al.

Cancer Res 2008;68:2233-2240.